AD-A074 071 DCW INDUSTRIES INC STUDIO CITY CA F/G 20/4
DEVELOPMENT OF AN ALTERNATIVE TO THE E9 PROCEDURE FOR PREDICTIN--ETC(U)
JUN 79 D C WILCOX N00014-78-C-0799
UNCLASSIFIED DCW-R-23-01 ONR-CR298-005-2F NL

END
DATE FILMED
10-79
DDC

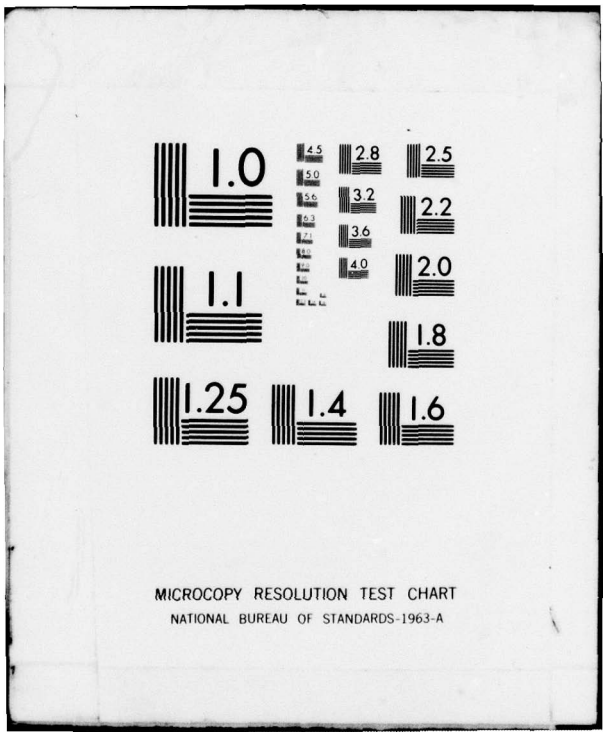
1.0
1.1
1.25
1.4
1.6
1.8
2.0
2.2
2.5
2.8
3.2
3.6
4.0
4.5
5.0
5.6
6.3
7.1
MICROCOPY RESOLUTION TEST CHART
NATIONAL BUREAU OF STANDARDS-1963-A

LEVEL II

REPORT ONR-CR298-005-2F

12 SL

DEVELOPMENT OF AN ALTERNATIVE TO THE E^9 PROCEDURE FOR PREDICTING BOUNDARY-LAYER TRANSITION

David C. Wilcox

DCW INDUSTRIES, INC.
Studio City
California
91604

CONTRACT N00014-78-C-0799
ONR TASK 298-005

June 1979

FINAL REPORT

PREPARED FOR THE

OFFICE OF NAVAL RESEARCH • 800 N. QUINCY ST. • ARLINGTON • VA • 22217

Change of Address

Organization receiving reports on the initial distribution list should confirm correct address. This list is located at the end of the report. Any change of address or distribution should be conveyed to the Office of Naval Research, Code 211, Arlington, VA 22217.

Disposition

When this report is no longer needed, it may be transmitted to other organizations. Do not return it to the originator or the monitoring office.

Disclaimer

The findings and conclusions contained in this report are not to be construed as an official Department of Defense or Military Department position unless so designated by other official documents.

Reproduction

Reproduction in whole or in part is permitted for any purpose of the United States Government.

UNCLASSIFIED

SECURITY CLASSIFICATION OF THIS PAGE (When Data Entered)

REPORT DOCUMENTATION PAGE	READ INSTRUCTIONS BEFORE COMPLETING FORM
1. REPORT NUMBER: ONR-CR298-005-2F	2. GOVT ACCESSION NO. / 3. RECIPIENT'S CATALOG NUMBER
4. TITLE (and Subtitle): DEVELOPMENT OF AN ALTERNATIVE TO THE E^9 PROCEDURE FOR PREDICTING BOUNDARY-LAYER TRANSITION	5. TYPE OF REPORT & PERIOD COVERED: FINAL REPORT, 15 SEPT 1978 — 14 MAR 1979
	6. PERFORMING ORG. REPORT NUMBER: DCW-R-23-01
7. AUTHOR(s): DAVID C. WILCOX	8. CONTRACT OR GRANT NUMBER(s): N00014-78-C-0799
9. PERFORMING ORGANIZATION NAME AND ADDRESS: DCW INDUSTRIES, INC. 4367 Troost Avenue Studio City, California 91604	10. PROGRAM ELEMENT, PROJECT, TASK AREA & WORK UNIT NUMBERS: 61153N RR023 01-83 NR298-005
11. CONTROLLING OFFICE NAME AND ADDRESS: PROGRAM OFFICE OF NAVAL RESEARCH, VEHICLE TECH. CODE 211, 800 North Quincy Street Arlington, Virginia 22217	12. REPORT DATE: JUNE 1979 / 13. NUMBER OF PAGES: 46
14. MONITORING AGENCY NAME & ADDRESS (if different from Controlling Office): 51 p.	15. SECURITY CLASS. (of this report): UNCLASSIFIED / 15a. DECLASSIFICATION/DOWNGRADING SCHEDULE

16. DISTRIBUTION STATEMENT (of this Report)

Approved for Public Release, Distribution Unlimited.

RR023 01 83

17. DISTRIBUTION STATEMENT (of the abstract entered in Block 20, if different from Report)

18. SUPPLEMENTARY NOTES

19. KEY WORDS (Continue on reverse side if necessary and identify by block number)

TRANSITION, TURBULENCE MODELING, LINEAR STABILITY THEORY

393 352

20. ABSTRACT (Continue on reverse side if necessary and identify by block number)

A method has been devised which can be used in conjunction with linear-stability theory for predicting boundary-layer transition. As with the classical "e^9" procedure, for a given frequency the growth of a disturbance is computed downstream of the initial point of instability using the linearized equations of motion. In contrast to the e^9 procedure in which the linearized equations are used all the way to the inferred transition point, an approximate set of long-time averaged equations which account for nonlinearity

DD FORM 1 JAN 73 1473 EDITION OF 1 NOV 65 IS OBSOLETE

UNCLASSIFIED

SECURITY CLASSIFICATION OF THIS PAGE (When Data Entered)

is used to describe the ultimate nonlinear growth of the disturbance. Because the new method accounts for nonlinear processes it holds promise as a more physically sound procedure than the e^9 method for determining the point at which a boundary layer undergoes transition to turbulence.

CONTENTS

LIST OF ILLUSTRATIONS

LIST OF ILLUSTRATIONS (Continued)

1. INTRODUCTION

The purpose of this research study has been to devise a physically sound alternative to the Smith[1] - Van Ingen[2] e^9 procedure for predicting boundary-layer transition. The need for developing an alternative procedure stems from the following: On the one hand, there is little doubt that stability theory's Tollmien-Schlichting waves exist and play an important role in the initial stages of transition. On the other hand, because the end state of the transition process is a (highly nonlinear) turbulent flow, linear-stability theory must break down at some point between that of the initiation of Tollmien-Schliehting waves and the transition point (defined, for example, as the point where skin friction achieves a minimum). In other words, linear-stability theory is inapplicable in the post-critical stages of transition and therefore has no natural way of specifying the actual transition point. The empirical e^9 method ignores this conceptual limitation and thus has a questionable physical foundation.

Under sponsorship of the Office of Naval Research (ONR), DCW Industries has taken an important first step toward developing a physically-sound alternative to the e^9 method for predicting transition. The basic approach has been to devise a synthesis of linear-stability theory and turbulence-model techniques by using each theory only in the regime where its inherent limitations determine its applicability. Our first step has consisted of showing that a key closure coefficient, λ, in the turbulence-model equations is relatively insensitive to frequency after a boundary-layer disturbance has been amplified to about e^4 times its initial value, provided the boundary layer is unstable.

While results of this first step have been very encouraging, analysis has been confined to the Blasius boundary layer,

primarily because of difficulties encountered in acquiring and debugging modifications to the Mack[3] stability program. Additional research has been needed to confirm our hypothesis that a linear-stability/turbulence-model synthesis is feasible. Specifically, two things need to be done. First, for the constant pressure case, actual transition predictions must be made using the stability-predicted λ profile and appropriate initial and boundary conditions. Second, computation of this key closure coefficient when the pressure varies is needed to provide a more stringent test of our hypothesis. Both ends have been accomplished in this research study.

Section 2 reviews the basic formulation underlying our theoretical approach. In Section 3, the Blasius boundary layer is analyzed including comparison of predicted and experimentally-measured transition points. Effects of both adverse and favorable pressure gradient are addressed in Section 4. Results and conclusions follow in Section 5.

2. THEORETICAL FORMULATION

In this section, for the sake of completeness, we first review the overall approach devised by Wilcox.[4] Then the turbulence model equations underlying the approach are presented. Finally, the manner in which turbulence-model parameters are computed from a given linear-stability solution is delineated.

2.1 OVERVIEW

Conceptually, our overall approach to predicting boundary-layer transition consists of three interrelated phases. In the first phase conventional linear-stability computations are performed up to and beyond the point at which a disturbance becomes unstable. As a key feature of these first-phase computations we have found empirically[4] that the computations are most appropriately terminated when the initial disturbance has been amplified by a factor of e^4. In the second phase the linear-stability solutions at the e^4-amplification point are used to compute key turbulence model parameters which are needed to specify the closure coefficient λ as well as initial and boundary conditions for a subsequent turbulence-model calculation. In the third phase a boundary-layer program incorporating the Wilcox-Traci[4-6] turbulence-model equations is used to predict the actual transition point. Most notably, a range of frequencies is considered in all phases of the computational procedure.

The rationale of this approach is two-fold. First, using linear-stability theory in the initial phase of the procedure allows us to take proper account of the transition phenomenon's sensitivity to the frequency of the disturbance. Using the turbulence-model equations is quite inappropriate in the initial phase as long-time averaging (which is an integral aspect of the turbulence-model theory) precludes explicit representation of frequency effects. Second, using the turbulence-model equations in the

final phase allows us (at least on a conceptual level) to represent nonlinear processes which ultimately must become dominant as the boundary layer nears transition to a turbulent state. Using linear-stability theory is quite inappropriate in the final phase as the linearization precludes explicit representation of nonlinear effects.

The astute reader will notice that a key premise is implicit in the rationale of our approach. Specifically, for this approach to work, it must be the case that either (a) the transition phenomenon is frequency independent beyond the e^4-amplification point or (b) a method exists whereby frequency effects can be explicitly expressed in the turbulence-model equations during the latter phases of transition. As will be demonstrated in this report, while the transition process is somewhat frequency dependent beyond the e^4-amplification point, this frequency dependence can indeed be explicitly expressed in the model equations.

The remainder of this section is devoted to a description of the turbulence-model equations and the manner in which key turbulence-model parameters are computed from a linear-stability solution.

2.2 TURBULENCE-MODEL EQUATIONS

The two-equation model of turbulence developed by Wilcox and Traci[5,6] is used in this study for predicting boundary-layer development during the latter phases of transition. For incompressible boundary layers this model consists of the long-time averaged conservation of mass and momentum equations and two additional rate equations. Denoting arc length and surface-normal distance by x and y with corresponding velocity components u and v, the four equations of motion for incompressible boundary layers are:

$$\frac{\partial u}{\partial x} + \frac{\partial v}{\partial y} = 0 \tag{1}$$

$$u\frac{\partial u}{\partial x} + v\frac{\partial u}{\partial y} = -\frac{dp}{dx} + \frac{\partial}{\partial y}\left[(\nu + \varepsilon)\frac{\partial u}{\partial y}\right] \tag{2}$$

$$u\frac{\partial e}{\partial x} + v\frac{\partial e}{\partial y} = \left\{\alpha^*\left|\frac{\partial u}{\partial y}\right| - \beta^*\omega\right\}e + \frac{\partial}{\partial y}\left[(\nu+\sigma^*\varepsilon)\frac{\partial e}{\partial y}\right] \tag{3}$$

$$u\frac{\partial \omega^2}{\partial x} + v\frac{\partial \omega^2}{\partial y} = \left\{\alpha\left|\frac{\partial u}{\partial y}\right| - \left[\beta+2\sigma\left(\frac{\partial \ell}{\partial y}\right)^2\right]\omega\right\}\omega^2 + \frac{\partial}{\partial y}\left[(\nu+\sigma\varepsilon)\frac{\partial \omega^2}{\partial y}\right] \tag{4}$$

where p is pressure and ν is kinematic viscosity. The quantity ε is kinematic eddy viscosity which is computed as the ratio of specific turbulent mixing energy, e, to turbulent dissipation rate, ω, i.e.,

$$\varepsilon = e/\omega \tag{5}$$

Also, ℓ is the turbulence length scale computed according to

$$\ell = e^{1/2}/\omega \tag{6}$$

Finally, the quantities α, α^*, β, β^*, σ and σ^* are closure coefficients whose values appropriate for turbulent flows have been found empirically[5] to be given by the following:

$$\left.\begin{aligned} &\beta = 3/20, \qquad \beta^* = 9/100 \\ &\sigma = 1/2, \qquad \sigma^* = 1/2 \\ &\alpha = \frac{1}{3}\left[1 - (1-\lambda)\exp\left(-Re_T/2\right)\right] \\ &\alpha^* = \frac{3}{10}\left[1 - (1-\lambda)\exp\left(-2Re_T\right)\right] \end{aligned}\right\} \tag{7}$$

Where Re_T is Reynolds number based on turbulence properties defined as

$$Re_T = e^{\frac{1}{2}}\ell/\nu \qquad (8)$$

and the quantity λ is an additional closure coefficient whose value has been found by Wilcox[6] to vary with freestream turbulence level, surface temperature and pressure gradient. For the Blasius boundary layer a value of $\lambda = 1/11$ has been found to yield transition-point predictions in reasonably close agreement with experimentally measured transition points.[5,6] Experience with the model equations[6] has shown that the model's ability to predict transition hinges most heavily upon the closure coefficient λ.

Equations (1)-(4) must be solved subject to boundary conditions at the surface, $y=0$, and at the boundary-layer edge, $y=\delta$, where δ is boundary-layer thickness. Prior studies have established that for perfectly-smooth surfaces (rough surfaces are not considered in this study), we must require

$$u = v = e = 0 \qquad \text{at } y = 0 \qquad (9)$$

and

$$\omega \to \frac{20}{\beta}\,\frac{\nu}{y^2} \qquad \text{as } y \to 0 \qquad (10)$$

Denoting conditions at the boundary-layer edge by subscript e, we must also require

$$u = U_e(x) \qquad \text{at } y = \delta \qquad (11)$$

while $e_e(x)$ and $\omega_e(x)$ must satisfy the following simplified equations:

$$\left.\begin{aligned} U_e \frac{de_e}{dx} &= -\beta^* \omega_e e_e \\ U_e \frac{d\omega_e^2}{dx} &= -\beta \omega_e^3 \end{aligned}\right\} \text{at } y = \delta \qquad (12)$$

2.3 COMPUTING TURBULENCE-MODEL PARAMETERS FROM A LINEAR-STABILITY SOLUTION

As stated in Subsection 2.1, before the turbulence-model phase of the computation can be initiated, initial and boundary conditions as well as the closure coefficient λ must be deduced from the linear-stability solution. To do so we must first note several important facts about the various turbulence-model parameters.

First of all, in order to define initial and boundary values for e and ω we note that Wilcox and Chambers[7] have defined these quantities in terms of the fluctuating vertical velocity, v', according to the following:

$$e = \frac{9}{4} \langle v'^2 \rangle \tag{13}$$

and

$$\omega = \frac{3\nu}{\beta^*} \frac{\langle (\partial v'/\partial y)^2 \rangle}{\langle v'^2 \rangle} \tag{14}$$

where $\langle\ \rangle$ denotes long-time average. As the linear-stability solution yields the instantaneous v' profile, Equations (13) and (14) are sufficient to determine e and ω profiles provided a suitable time-averaging process can be defined.

Next, in order to determine λ, we first rewrite Equation (3) under the standard parallel-flow assumption (i.e., $v \equiv 0$) and in the limit of small turbulent Reynolds number (i.e., $Re_T << 1$). The result is †

$$u \frac{\partial e}{\partial x} = \frac{3}{10} \lambda \left| \frac{\partial u}{\partial y} \right| e - \beta^* \omega e + \nu \frac{\partial^2 e}{\partial y^2} \tag{15}$$

---

† Note that in the actual turbulence-model phase of the computation, Equation (3) is used. Equation (15) has been introduced only to devise a method for computing λ from the linear-stability solution.

Now, noting the definition of e given in Equation (13), we can derive an exact equation for its evolution by taking the v' moment of the v-momentum equation and time averaging. Assuming that in the limit $Re_T \to 0$ the triple correlation term is negligibly small, we obtain

$$u \frac{\partial e}{\partial x} = - \frac{9}{2} \left\langle \frac{v'}{\rho} \frac{\partial p'}{\partial y} \right\rangle - \frac{9}{2} \nu \left\langle \left(\frac{\partial v'}{\partial y} \right)^2 \right\rangle + \nu \frac{\partial^2 e}{\partial y^2} \qquad (16)$$

Comparison of Equations (15) and (16) shows that the closure coefficient λ can be defined as follows:

$$\lambda = \frac{10}{3} \frac{\nu \left\langle \left(\frac{\partial v'}{\partial y} \right)^2 \right\rangle - 2 \left\langle \frac{v'}{\rho} \frac{\partial p'}{\partial y} \right\rangle}{\langle v'^2 \rangle \left| \partial u / \partial y \right|} \qquad (17)$$

The final step in relating the linear-stability and the turbulence-model parameters is to define an appropriate long-time average. To do so we note first that in the linear-stability solution the velocity and pressure fluctuations, v' and p', are written as

$$v'(x,y,z,t) = U_\infty \, \phi(y) \, \exp \left[i \left(\hat{\alpha} x + \hat{\beta} z - \hat{\omega} t \right) \right] \qquad (18)$$

$$p'(x,y,z,t) = \rho U_\infty^2 \pi(y) \exp \left[i \left(\hat{\alpha} x + \hat{\beta} z - \hat{\omega} t \right) \right] \qquad (19)$$

where t denotes time, z is distance normal to the x and y axes, U_∞ is freestream velocity, ρ is density, $\hat{\alpha}$ and $\hat{\beta}$ are wave numbers, $\hat{\omega}$ is frequency, and the functions ϕ (y) and π (y) are the complex amplitude functions of the fluctuating flow variables v' and p'.

To evaluate the time-averaged quantities appearing in Equations (13), (14) and (17) we use the following definition:

$$\langle \psi \rangle = \lim_{\hat{\omega} T \to \infty} \frac{1}{2T} \int_{t-T}^{t+T} \psi(x,y,z,\tau) \, d\tau \qquad (20)$$

Then, working with the real parts of the linear-stability solution, performing all time averages indicated in Equations (13), (14) and (17), and denoting local Reynolds number by R yields the following:

$$e/U_\infty^2 = \frac{9}{8}\left(\phi_r^2 + \phi_i^2\right) \tag{21}$$

$$\frac{\nu\omega}{U_\infty^2} = \frac{3}{\beta^* R^2} \frac{(d\phi_r/d\eta)^2 + (d\phi_i/d\eta)^2}{\left(\phi_r^2 + \phi_i^2\right)} \tag{22}$$

$$\lambda = \frac{10}{3} \frac{R^{-1}\left[(d\phi_r/d\eta)^2 + (d\phi_i/d\eta)^2\right] - 2\left[\phi_r d\pi_r/d\eta + \phi_i d\pi_i/d\eta\right]}{\left(\phi_r^2 + \phi_i^2\right)\ |\partial U/\partial\eta|} \tag{23}$$

where $U \equiv u/U_\infty$, subscripts r and i denote real and imaginary parts, and η is dimensionless distance defined by

$$\eta \equiv y\sqrt{\frac{U_e}{\nu x}} \tag{24}$$

with U_e denoting horizontal velocity at the boundary-layer edge. Note that for the constant-pressure case, $U_e = U_\infty$. Equations (21)-(23) are the desired relations which can be used to define λ and the initial and boundary conditions for a turbulence-model computation in terms of a given linear-stability solution.

3. RESULTS FOR CONSTANT PRESSURE

In this section we implement the basic method for the constant-pressure case, i.e., for the Blasius boundary layer. First, we compute the closure coefficient λ for a range of frequencies and demonstrate that beyond the e^4-amplification point λ asymptotes to a nearly frequency-independent profile. Next, we compute e and ω profiles at the e^4-amplification point which can be used to initiate a turbulence-model computation. Then, we establish boundary conditions for the turbulence-model phase. Finally, transition predictions are made and compared with experimental data.

3.1 EVALUATION OF THE CLOSURE COEFFICIENT λ

Using Equation (17), Wilcox[4] has computed λ profiles for the Blasius boundary layer. For the sake of completeness results obtained in the Wilcox study are repeated in this subsection.

A large number of linear-stability computations have been performed with the Mack[3] stability program; all computations have been done with the spatial amplification theory option. Both Reynolds number and frequency have been varied in order to determine the variation of λ throughout the Reynolds-number/frequency plane.

Figure 1 shows computed λ profiles at nine Reynolds numbers corresponding to one stable case, one neutrally-stable case, and seven unstable cases corresponding to amplification from the neutral case by factors of e^n with values of n ranging 0 to 10; for all nine cases the frequency is given by

$$Fr = \hat{\omega}\nu/U_\infty^2 = 2\cdot 10^{-5} \qquad (25)$$

We are thus following the evolution of λ for a constant-frequency disturbance at a Reynolds number upstream of the neutral point corresponding to the frequency given in Equation (25).

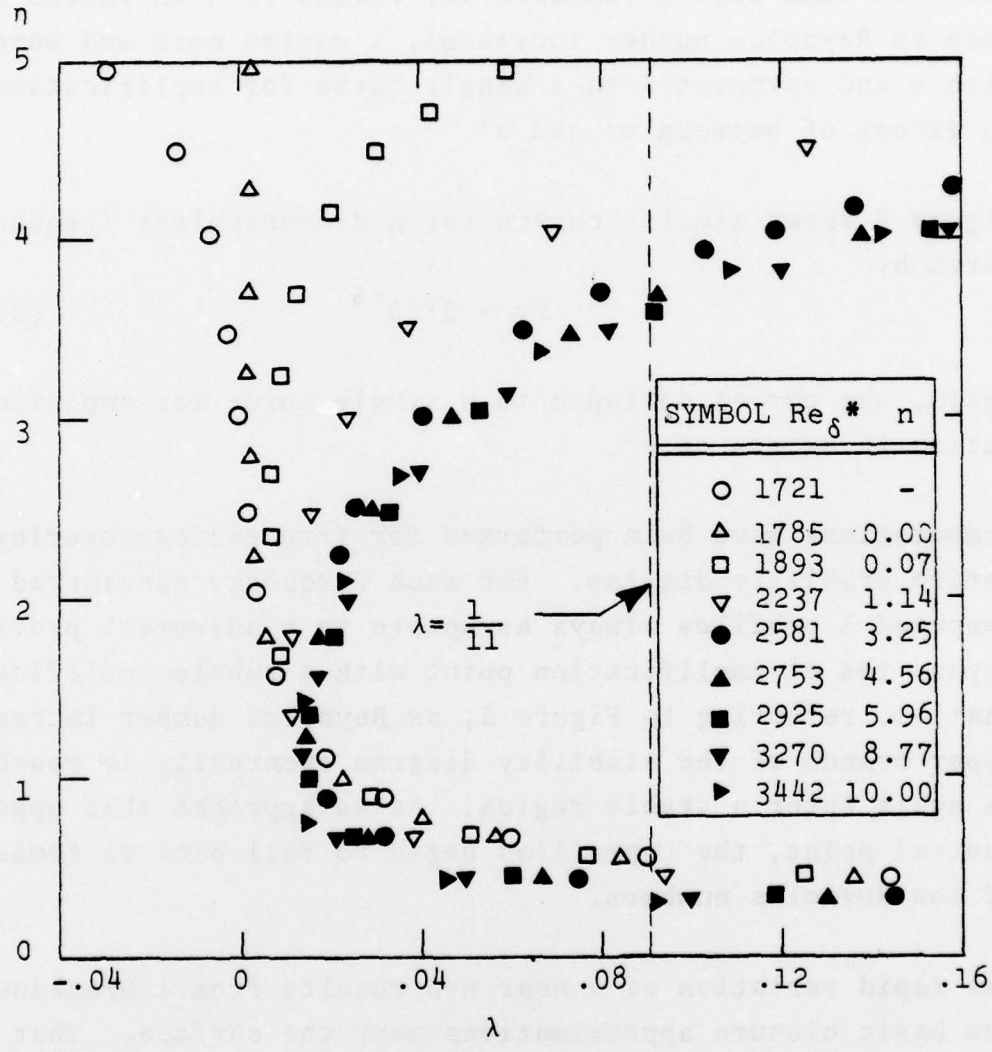

Figure 1. Computed λ profiles for dimensionless frequency Fr = $2 \cdot 10^{-5}$; zero pressure gradient.

As shown, although λ varies rapidly with y near the surface, all nine curves display approximately the same variation. However, above a value of $\eta=2$, the various λ profiles vary rapidly with η and do so in dissimilar manner for amplification rates up to $e^{4.56}$. For example, at the lowest Reynolds number for which the solution is stable, λ is negative above $\eta=2$. As we move to the neutral point we find that λ vanishes for values of η in excess of 2.5. Then as Reynolds number increases, λ varies more and more rapidly with η and asymptotes to a single curve for amplification ratios in excess of between e^3 and e^4.

Figure 2 shows similar curves for a dimensionless frequency Fr given by

$$Fr = 3 \cdot 10^{-5} \qquad (26)$$

Again, the curves collapse to a single curve for amplification ratios in excess of e^4.

Computations have been performed for frequencies covering the entire stability diagram. For each frequency considered the computed λ profiles always asymptote to a universal profile beyond the e^4-amplification point with a subtle qualification. That is, referring to Figure 3, as Reynolds number increases the upper branch of the stability diagram eventually is reached and we again enter a stable region. As we approach this upper neutral point, the λ proflies begin to fall back to those typical of low Reynolds numbers.

The rapid variation of λ near $\eta=0$ results from a breakdown in the basic closure approximations near the surface. That is, the the production term in the $\langle v'^2 \rangle$ equation, $\langle -\frac{v'}{\rho}\frac{\partial p'}{\partial y} \rangle$, goes to zero quadratically with distance from the surface so that, in terms of η,

$$\left\langle -\frac{v'}{\rho}\frac{\partial p'}{\partial y} \right\rangle \sim \eta^2 \qquad \text{as} \quad \eta \to 0 \qquad (27)$$

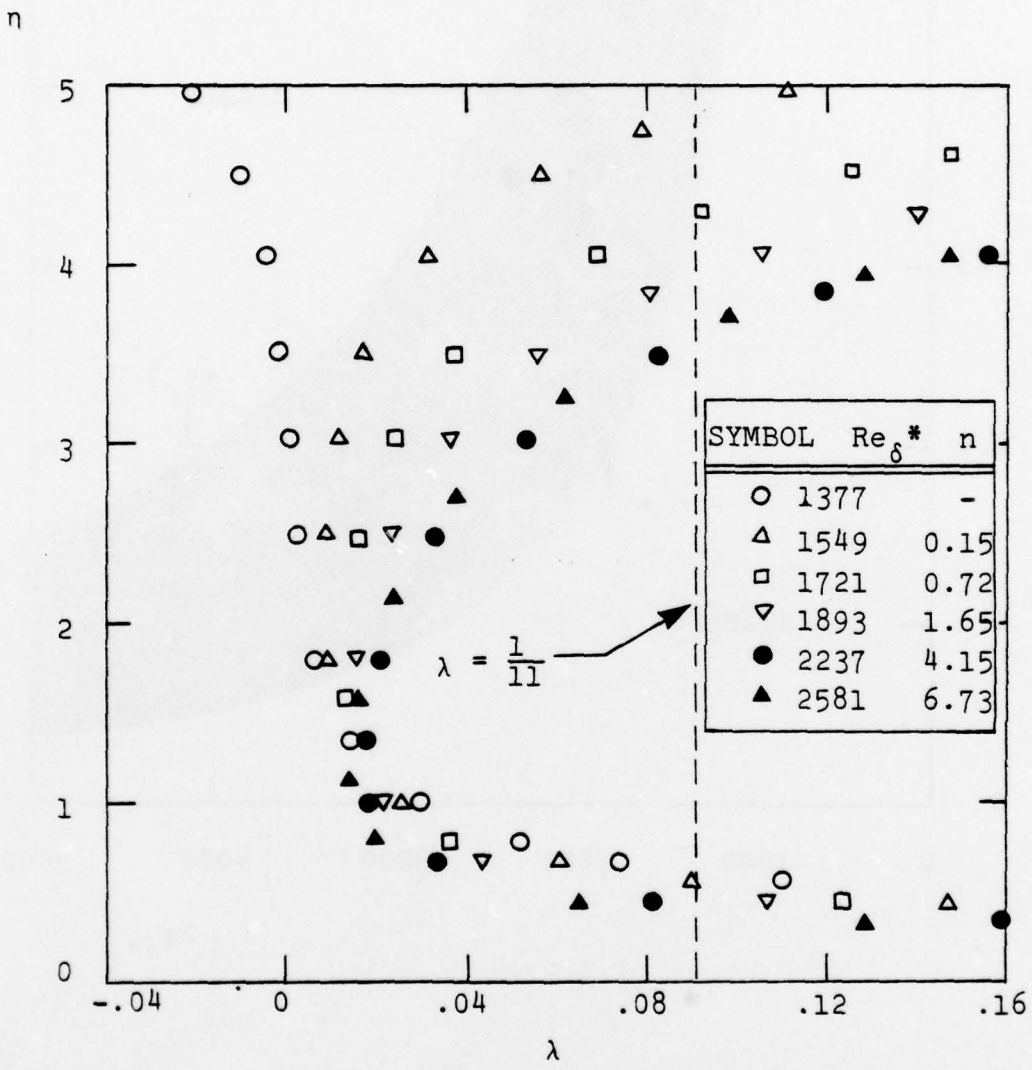

Figure 2. Computed λ profiles for dimensionless frequency Fr = $3 \cdot 10^{-5}$; zero pressure gradient.

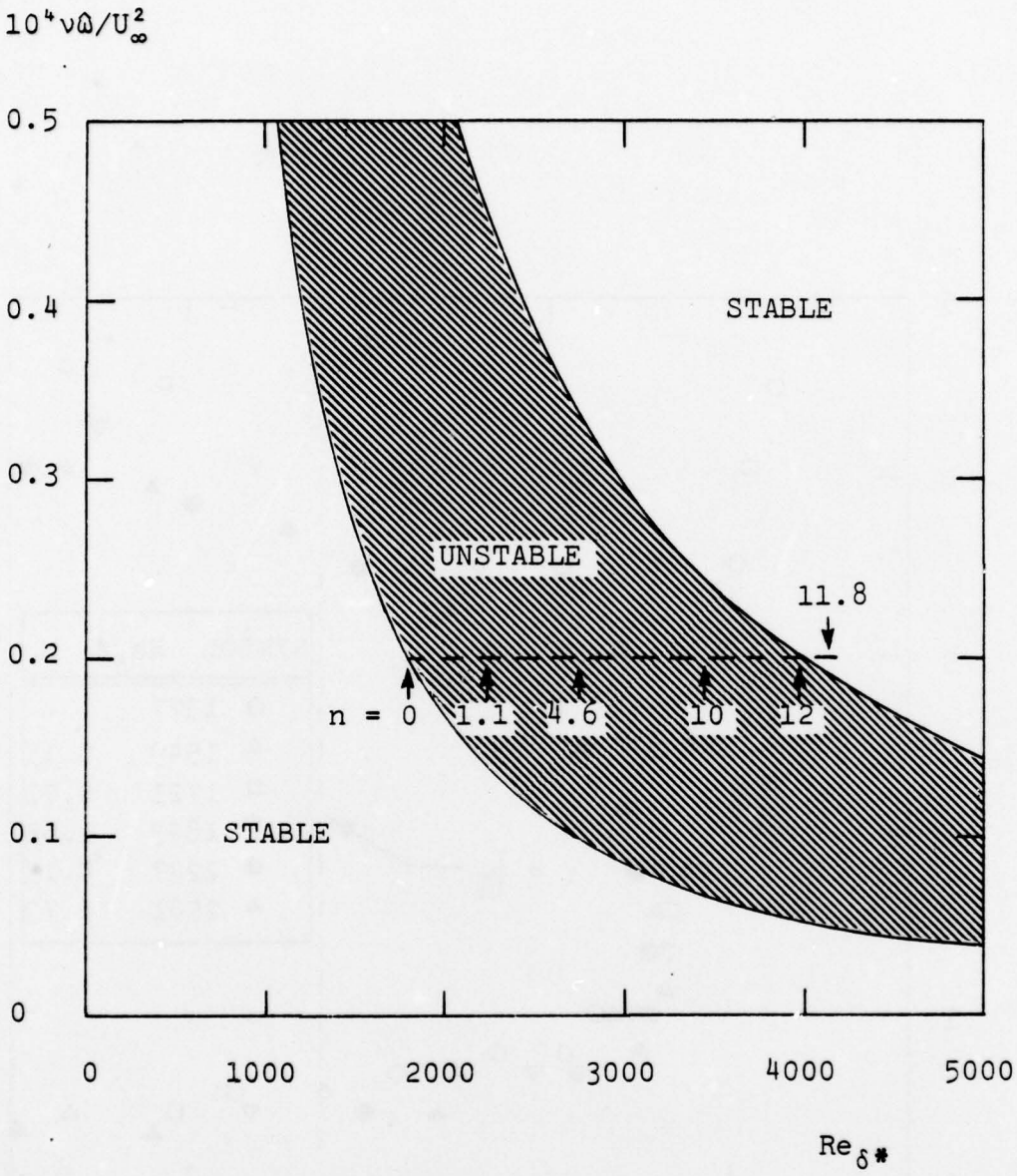

Figure 3. Stability diagram for the Blasius boundary layer depicting a constant frequency trajectory; n denotes solution amplification of e^n.

By contrast, the modeled production term for $Re_T \to 0$ behaves as

$$\frac{3}{10} \lambda \frac{\partial u}{\partial y} e \sim \lambda \eta^4 \qquad \text{as} \quad \eta \to 0 \qquad (28)$$

Consequently, close to the surface we have

$$\lambda \sim \eta^{-2} \qquad \text{as} \quad \eta \to 0 \qquad (29)$$

This modeling shortcoming is of little consequence as dissipation exceeds production near $\eta=0$. Hence, for the remainder of this discussion our focus will be upon the region between $\eta=1$ and the outer edge of the boundary layer, $\eta=5$.

Figure 4 shows computed λ profiles for several frequencies and amplification ratios. As shown, all of the computed λ profiles cluster about the approximate profile defined by

$$\lambda = .0093 + .00156 \exp\left[\frac{10}{7}(\eta-1)\right] \qquad (30)$$

The fact that the computed λ profiles correlate with the profile defined in Equation (30) independent of frequency is extremely important. This is our first indication that using the turbulence-model equations to describe the latter stages of transition is feasible.

It is interesting to examine the rate of approach to the asymptotic profile which is most conveniently done in terms of the average value of λ defined as follows:

$$\bar{\lambda} \equiv \frac{1}{4}\int_1^5 \lambda \, d\eta \qquad (31)$$

Figure 5 shows $\bar{\lambda}$ as a function of displacement thickness Reynolds number, Re_{δ^*}; note that $Re_{\delta^*_{\frac{1}{7}}}$ denotes the neutral-stability value of Re_{δ^*} for a given frequency. As shown, for the higher

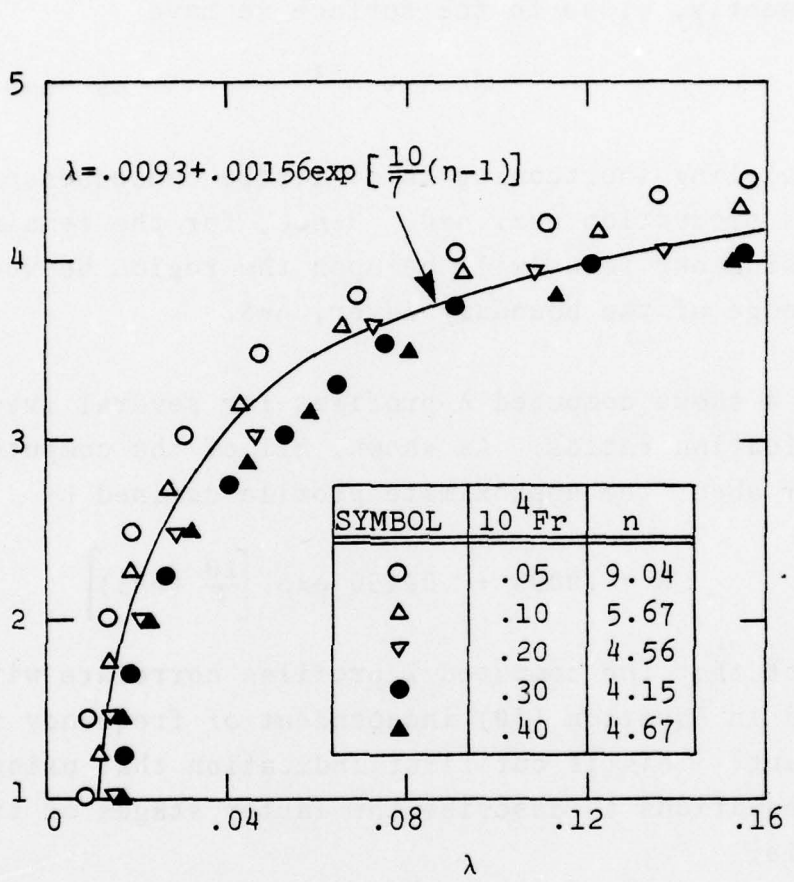

Figure 4. Profiles of the closure coefficient λ for various frequencies and amplification ratios; zero pressure gradient.

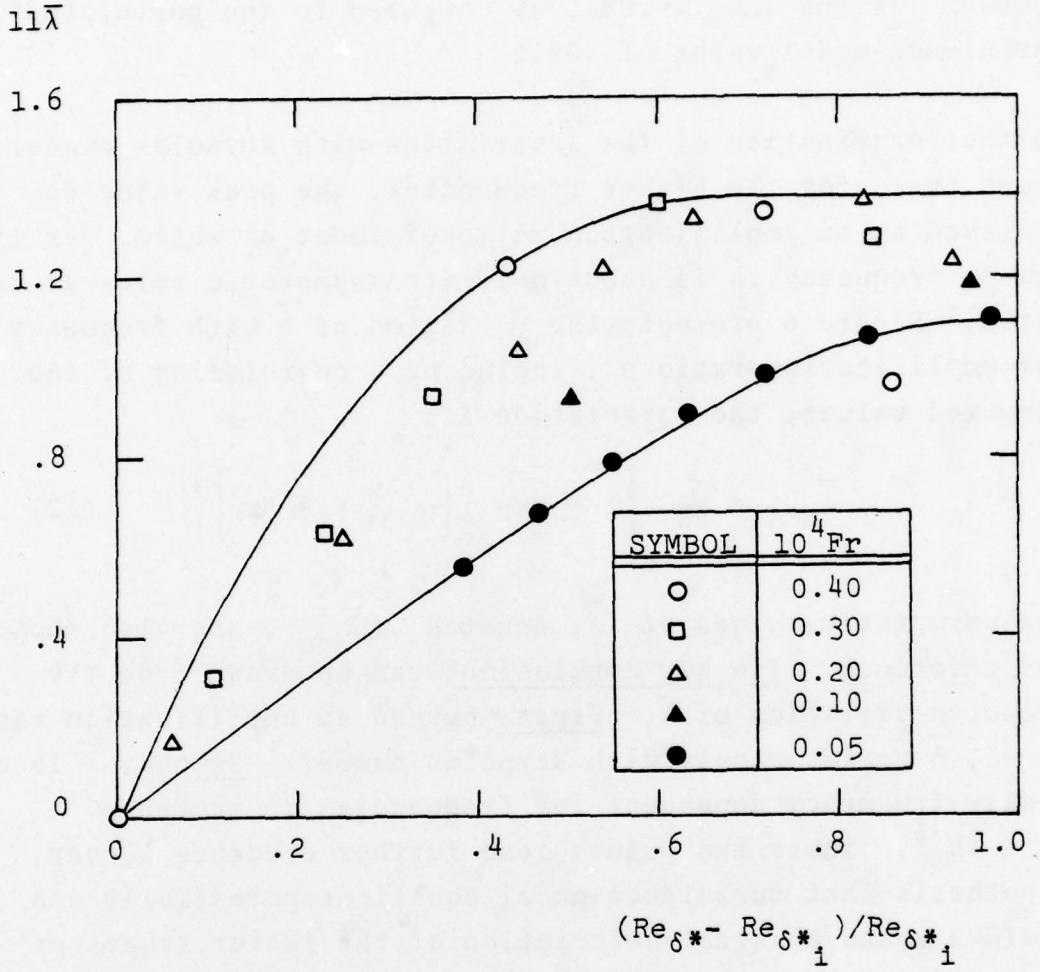

Figure 5. Variation of $\overline{\lambda}$ with Reynolds number for several frequencies; zero pressure gradient.

frequencies $\bar{\lambda}$ approaches its asymptotic value most rapidly. For Fr = $0.5 \cdot 10^{-5}$, the lowest frequency at which computations have been done, the approach to the asymptotic values lie between $\bar{\lambda}$=.066 and $\bar{\lambda}$=.083, as compared to the postulated[6] turbulence-model value of .091.

Further examination of the $\bar{\lambda}$ variation with Reynolds number shows that, for the higher frequencies, the peak value is achieved at an amplification ratio of about e^4 while, for the lowest frequency, $\bar{\lambda}$ is about half its asymptotic value at this ratio. Figure 6 presents the variation of $\bar{\lambda}$ with frequency for amplification ratio e^4, including a correlation of the computed values; the correlation is:

$$\bar{\lambda}_{n=4} = \frac{7}{55} \left\{1 - \exp \left[- \frac{25}{3} (10^4 \mathrm{Fr})\right]\right\} \qquad (32)$$

The asymptotic values of $\bar{\lambda}$, denoted as $\bar{\lambda}_{max}$, are also shown for reference. Two key conclusions can be drawn from the computed variation of $\bar{\lambda}$. First, beyond an amplification ratio of e^4, $\bar{\lambda}$ varies slowly with Reynolds number. Second, $\bar{\lambda}$ is only weakly frequency dependent for frequencies in excess of Fr = 10^{-5}. These two points lend further credence to our hypothesis that turbulence-model equations potentially can yield a sound physical description of the latter stages of transition.

3.2 INITIAL PROFILES

Having established Equation (30) as a satisfactory correlation of computed $\bar{\lambda}$ profiles we now turn to initial profiles for e and ω which are needed to initiate a boundary-layer computation beyond the e^4-amplification point. Figures 7 and 8 show computed profiles for e and ω at the e^4-amplification point. These profiles have been obtained from the linear-stability

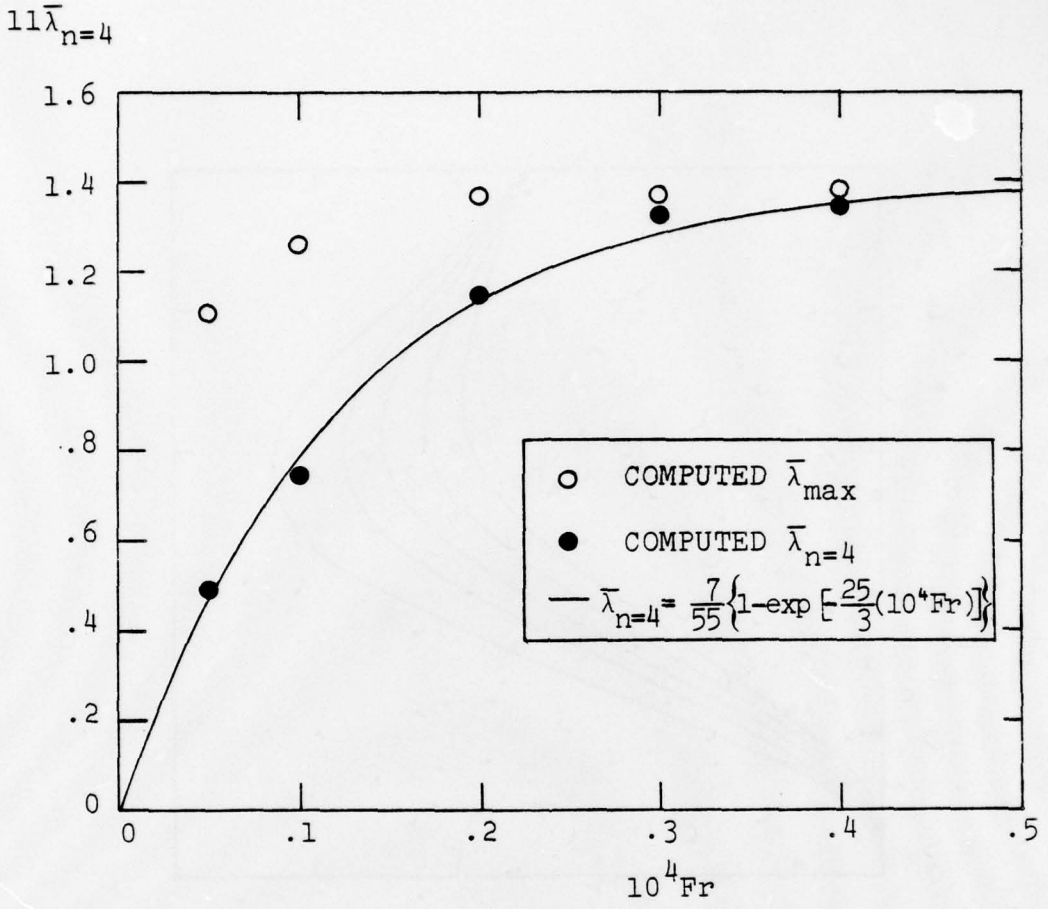

Figure 6. Correlation of the average value of λ with frequency for an amplification ratio of e^4; zero pressure gradient.

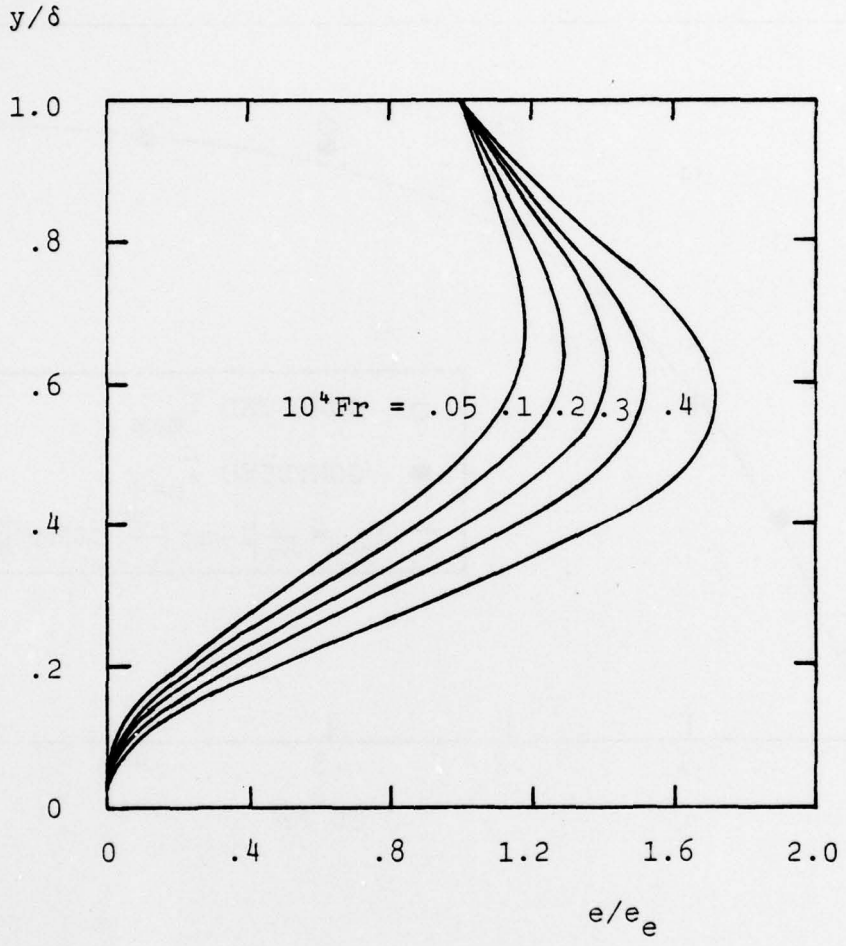

Figure 7. Computed turbulent mixing-energy profiles after an initial disturbance has been amplified by a factor of e^4; zero pressure gradient.

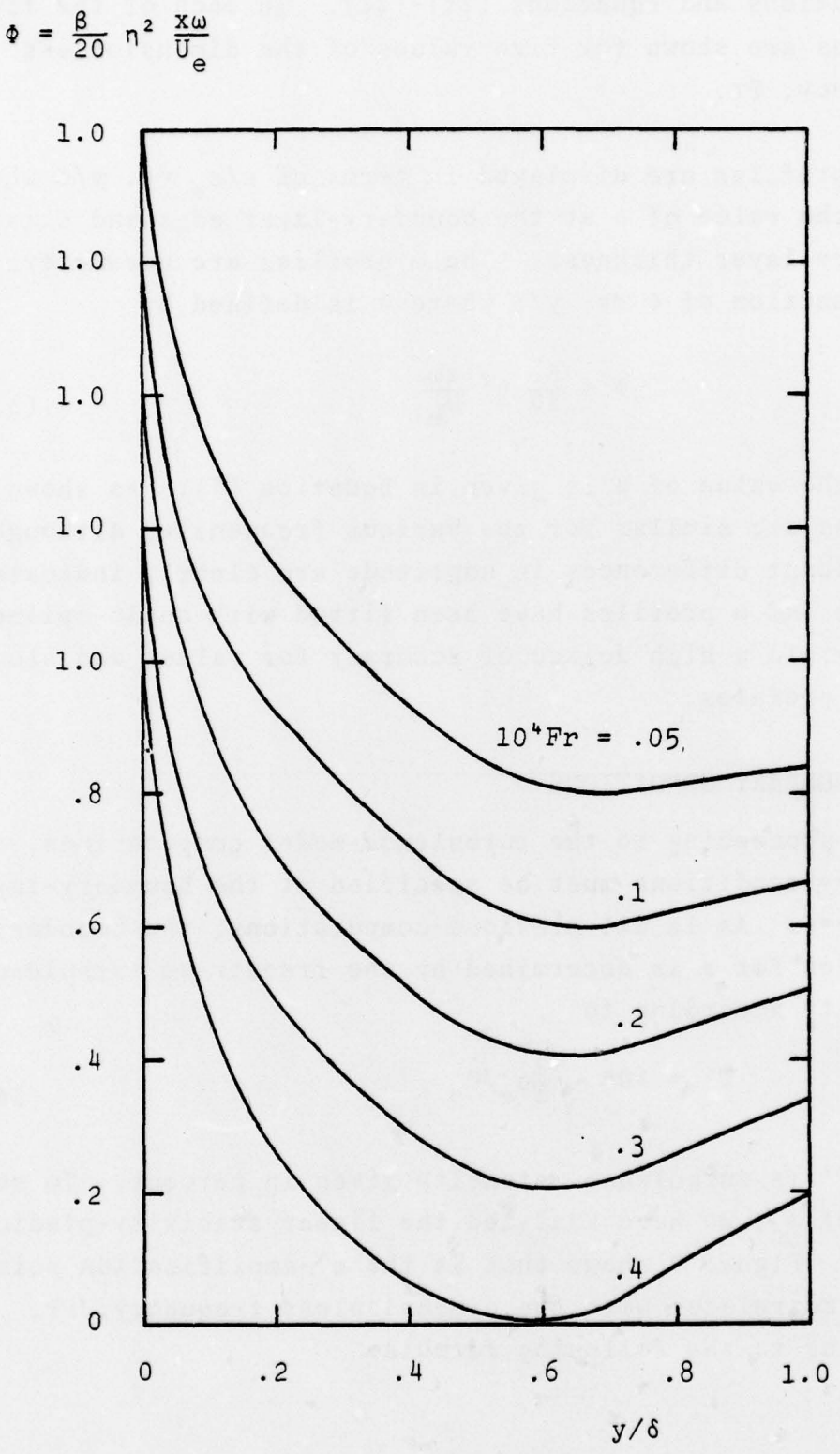

Figure 8. Computed turbulent dissipation-rate profiles after an initial disturbance has been amplified by a factor of e^4; zero pressure gradient.

computations and Equations (21)-(22). In each of the figures profiles are shown for five values of the dimensionless frequency, Fr.

The e profiles are displayed in terms of e/e_e vs. y/δ where e_e is the value of e at the boundary-layer edge and δ is boundary-layer thickness. The ω proflies are parameterized as a function of Φ vs. y/δ where Φ is defined by

$$\Phi = \frac{\beta}{20} \eta^2 \frac{x\omega}{U_e} \tag{33}$$

where the value of β is given in Equation (7). As shown, the profiles are similar for the various frequencies although significant differences in amplitude are clearly indicated. These e and ω profiles have been fitted with cubic splines which yield a high degree of accuracy for values and slopes of the profiles.

3.3 BOUNDARY CONDITIONS

Before proceeding to the turbulence-model computations, boundary-conditions must be specified at the boundary-layer edge, $y=\delta$. As in all previous computations, the boundary condition for e is determined by the freestream turbulence intensity according to

$$T' = 100 \sqrt{\frac{2}{3} e_e / U_e} \tag{34}$$

where T' is turbulence intensity given in percent. To set the value of ω_e, we have analyzed the linear-stability-predicted values. Figure 9 shows that at the e^4-amplification point, $\nu\omega_e/U_e^2$ correlates with the dimensionless frequency, Fr, according to the following formula:

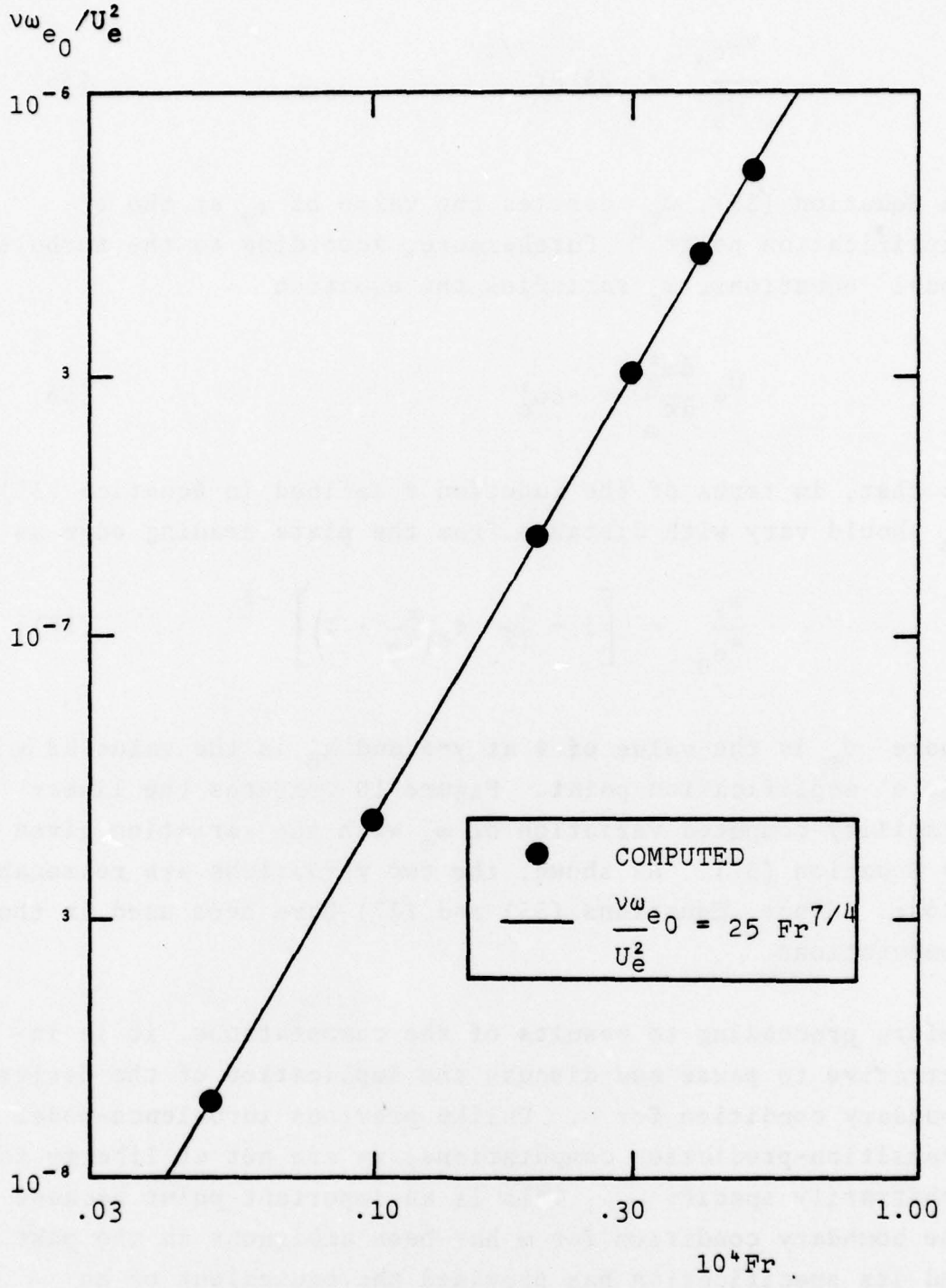

Figure 9. Correlation of boundary-layer-edge value of the turbulent dissipation rate with dimensionless frequency; zero pressure gradient.

$$\frac{\nu\omega_{e_0}}{U_e^2} = 25\ Fr^{7/4} \qquad (35)$$

In Equation (35), ω_{e_0} denotes the value of ω_e at the e^4-amplification point. Furthermore, according to the turbulence model equations, ω_e satisfies the equation

$$U_e \frac{d\omega_e^2}{dx} = -\beta\omega_e^3 \qquad (36)$$

so that, in terms of the function Φ defined in Equation (33), ω_e should vary with distance from the plate leading edge as

$$\frac{\omega_e}{\omega_{e_0}} = \left[1 + \frac{5}{18}\ \Phi_e\left(\frac{x}{x_0} - 1\right)\right]^{-1} \qquad (37)$$

where Φ_e is the value of Φ at $y=\delta$ and x_0 is the value of x at the e^4-amplification point. *Figure 10 compares the linear-stability-computed variation of* ω_e with the variation given by Equation (37). As shown, the two variations are reasonably close. Hence, Equations (35) and (37) have been used in the computations.

Before proceeding to results of the computations, it is instructive to pause and discuss the implication of the derived boundary condition for ω. Unlike previous turbulence-model transition-prediction computations, we are not at liberty to arbitrarily specify ω_e. This is an important point because the boundary condition for ω has been ambiguous in the past and its specification has provided the equivalent of an "adjustable parameter" in the theory. Elimination of this adjustability enhances utility of the method, particularly if it proves to be an accurate predictive tool.

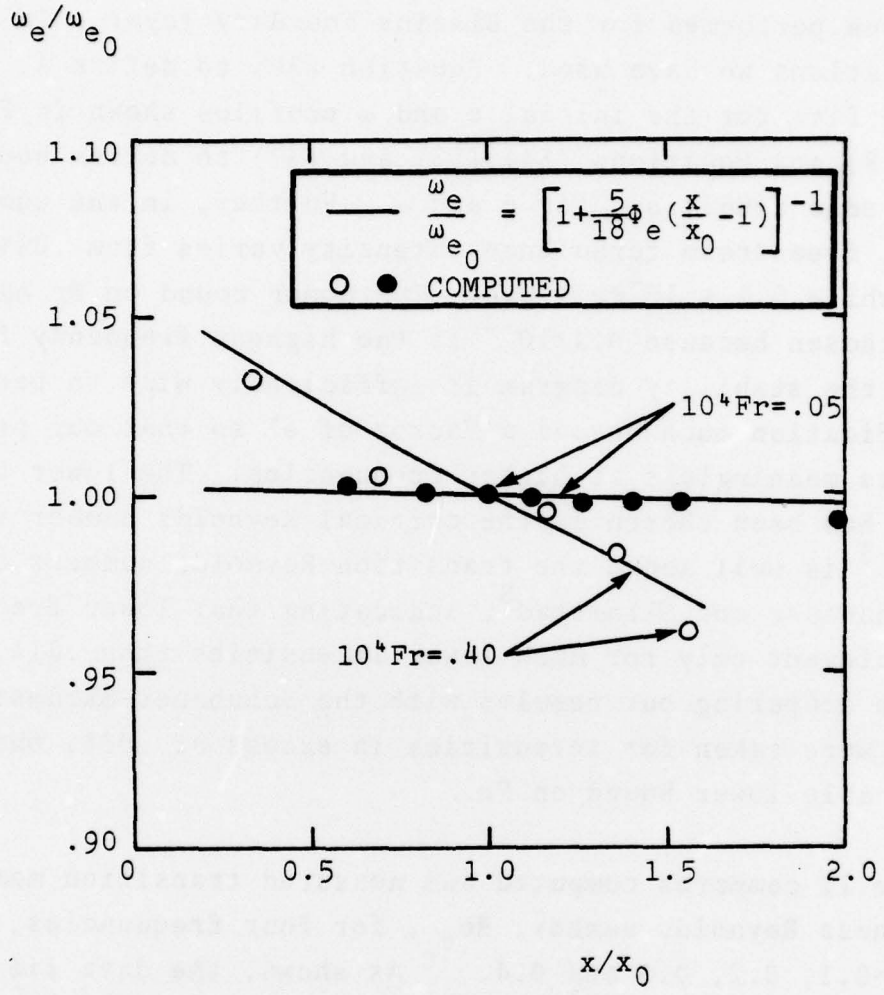

Figure 10. Comparison of linear-stability-computed variation of ω_e with model-equation-predicted variation; zero pressure gradient.

3.4 TRANSITION PREDICTIONS

To assess the accuracy of the method, a series of computations has been performed for the Blasius boundary layer. In all calculations we have used: Equation (30) to define λ; cubic spline fits for the initial e and ω profiles shown in Figures 7 and 8; and Equations (34),(35) and (37) to define boundary-layer edge conditions for e and ω. Further, in the computations, freestream turbulence intensity varies from .01% to .50% while $0.1 < 10^4 Fr < 0.4$. The upper bound on Fr has been chosen because $0.4 \cdot 10^{-4}$ is the highest frequency for which the stability diagram is sufficiently wide to permit amplification much beyond a factor of e^4 so that our procedure becomes meaningless at higher frequencies. The lower bound on Fr has been chosen as the critical Reynolds number for $Fr=10^{-5}$ is well above the transition Reynolds numbers observed by Schubauer and Skramstad[8], indicating that lower frequencies are relevant only for much lower intensities than .01%. Since we are comparing our results with the Schubauer-Skramstad data which were taken for intensities in excess of .02%, this is a reasonable lower bound on Fr.

Figure 11 compares computed and measured transition momentum-thickness Reynolds number, Re_{θ_t}, for four frequencies, viz, $10^4 Fr=0.1$, 0.2, 0.3 and 0.4. As shown, the data lie mostly near the curves for $10^4 Fr=0.2$ and 0.4. This result is quite encouraging as this band of frequencies is comparable to that predicted by linear-stability theory[3] to be most unstable for the range of transition Reynolds numbers observed by Schubauer and Skramstad.

Figure 12 compares computed and measured transition Reynolds number based on distance from the plate leading edge, Re_{x_t}; only the curve computed with $10^4 Fr=0.2$ is shown for simplicity. This figure displays an interesting feature of

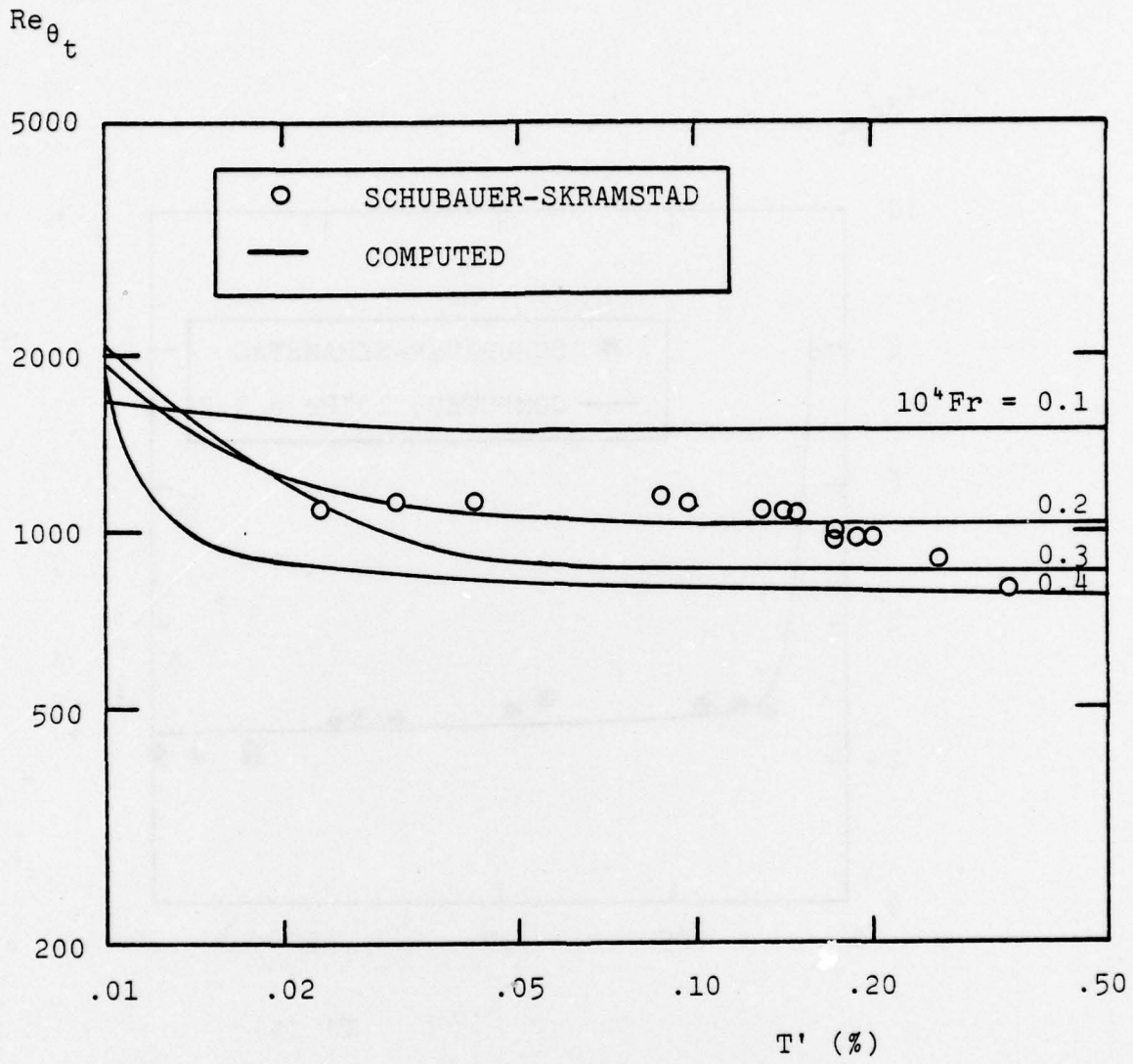

Figure 11. Comparison of computed and measured transition momentum-thickness Reynolds number for the Blasius boundary layer.

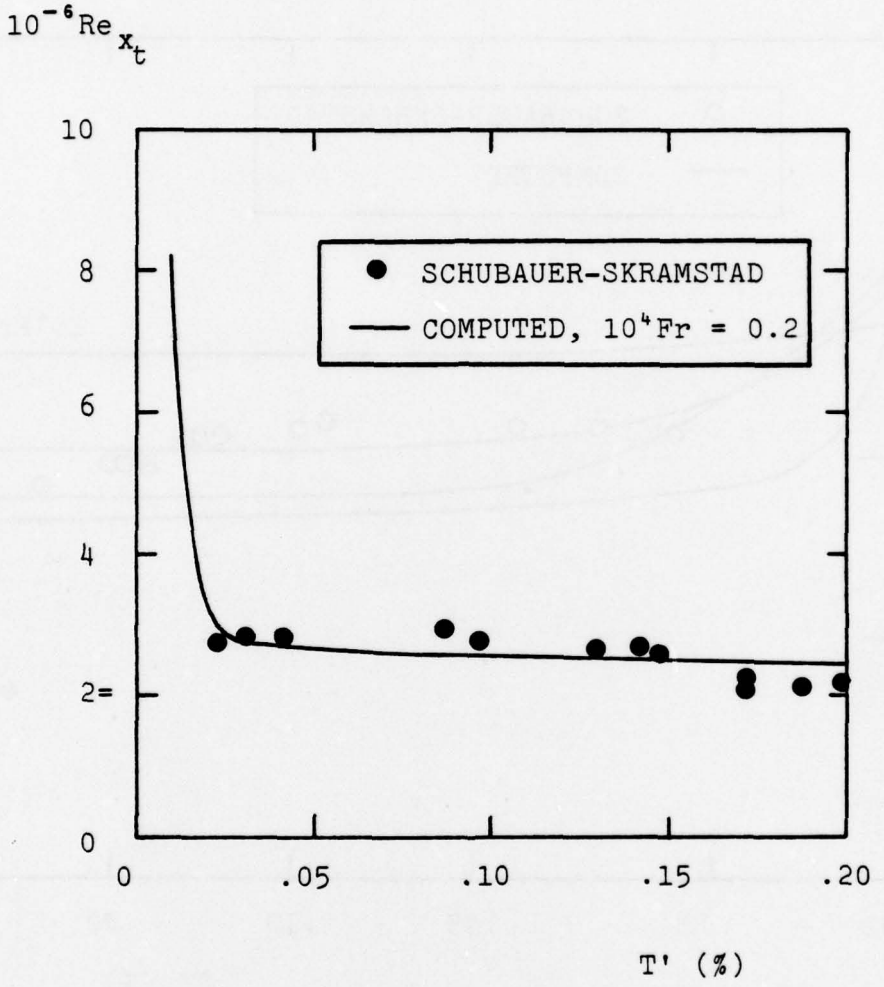

Figure 12. Comparison of computed and measured transition plate-length Reynolds number for the Blasius boundary layer.

the computations, viz, that following the predicted variation of Re_{x_t} with T' down to about T'=.03% indicates an asymptote to a finite value of Re_{x_t} as T'→0, similar to the trend of the data. However below T'=.03%, the predicted Re_{x_t} then increases rapidly implying that Re_{x_t} may approach an infinite value as T' → 0. Although not shown in the figure, a similar trend appears for the other frequencies.

As evidence of the method's ability to properly treat spectral effects, Figure 13 compares an inferred "most-dangerous" frequency with the linear-stability-theory predicted "most-dangerous" frequency band. The inferred curve has been constructed by forcing agreement between model-predicted transition point and the Schubauer-Skramstad data. As shown, the curve lies just slightly outside the linear-stability-theory band.

As a final note, the actual transition predictions have been found to be relatively insensitive to initial profiles. To make a similar claim about whether starting the turbulence-model computation at a different point (e.g., when the amplification ratio is e^3 or e^5) would require further research. Some computations have been done from the e^5-amplification point and this appeared to have little effect on the predicted transition point.

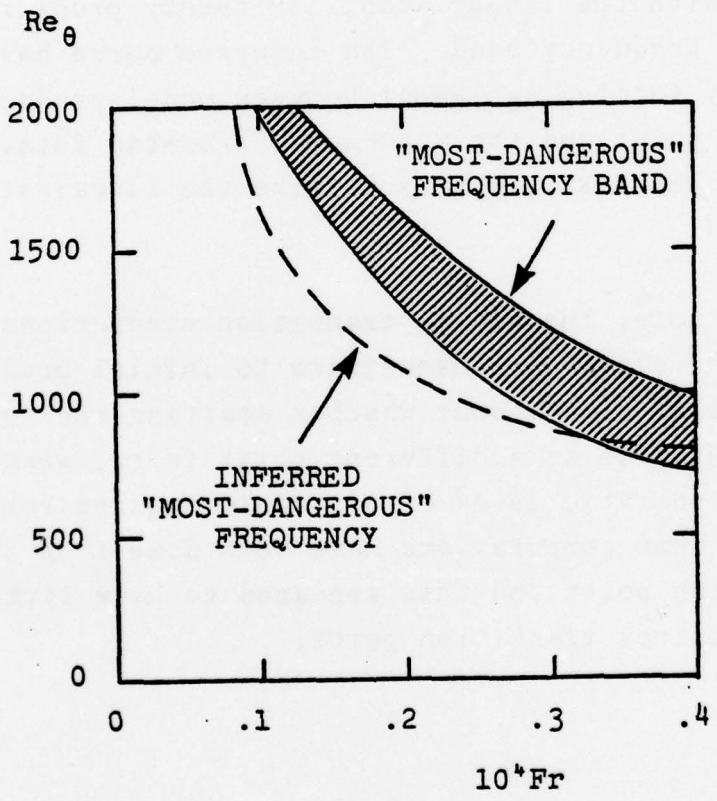

Figure 13. Spectral effects.

4. EFFECTS OF PRESSURE GRADIENT

In order to investigate effects of pressure gradient, we now repeat the analysis of Section 3 using Falkner-Skan velocity profiles for both adverse and favorable pressure gradients. First, we compute λ profiles at the e^4-amplification point and seek a frequency-independent correlation. Then the boundary-layer edge condition for ω is correlated with frequency. Results follow.

4.1 EVALUATION OF THE CLOSURE COEFFICIENT λ

The Falkner-Skan profiles satisfy the following equation:

$$\frac{d^3f}{d\tilde{\eta}^3} + f\frac{d^2f}{d\tilde{\eta}^2} + \beta_{FS}\left[1 - \left(\frac{df}{d\tilde{\eta}}\right)^2\right] = 0 \qquad (38)$$

which is solved subject to:

$$\left.\begin{aligned} f = \frac{df}{d\tilde{\eta}} = 0 \quad &\text{at} \quad \tilde{\eta}=0 \\ \frac{df}{d\tilde{\eta}} \to 1 \quad &\text{as} \quad \tilde{\eta}\to\infty \end{aligned}\right\} \qquad (39)$$

In Equation (38), f is the dimensionless streamfunction so that the velocity u is obtained from

$$u = U_e \frac{df}{d\tilde{\eta}} \qquad (40)$$

Also, the freestream velocity, U_e, is given by

$$U_e(x) = Cx^m \qquad (41)$$

where C is a constant and m is related to the constant β_{FS} appearing in Equation (38) through the following equation:

$$\beta_{FS} = \frac{2m}{m+1} \tag{42}$$

Finally, the scaled coordinate $\tilde{\eta}$ is defined in terms of x,y,ν and U_e by

$$\tilde{\eta} = y\sqrt{\frac{m+1}{2}\frac{Ue}{\nu x}} \tag{43}$$

Note that for zero pressure gradient m=0 and Equation (43) differs from Equation (24) by a factor $\sqrt{2}$. For the sake of consistency with our earlier computations, all results in this section are cast in terms of η as defined in Equation (24) rather than in terms of $\tilde{\eta}$.

For symmetry, we consider one adverse pressure gradient profile and one favorable pressure gradient profile, viz, we select

$$\beta_{FS} = \begin{cases} -0.18 \text{ , adverse } \nabla p \\ +0.18 \text{ , favorable } \nabla p \end{cases} \tag{44}$$

which correspond to m=-.083 and m=+.099 for the adverse and favorable cases, respectively.

Turning first to adverse pressure gradient, Figure 14 shows computed values of λ for several frequencies near the e^4-amplification point; the correlation for zero pressure gradient [Equation (30)] is shown for reference. As can be seen, the various λ profiles show a stronger frequency dependence than exists in the absence of pressure gradient. Furthermore, the disparity in the various profiles fails to diminish as η

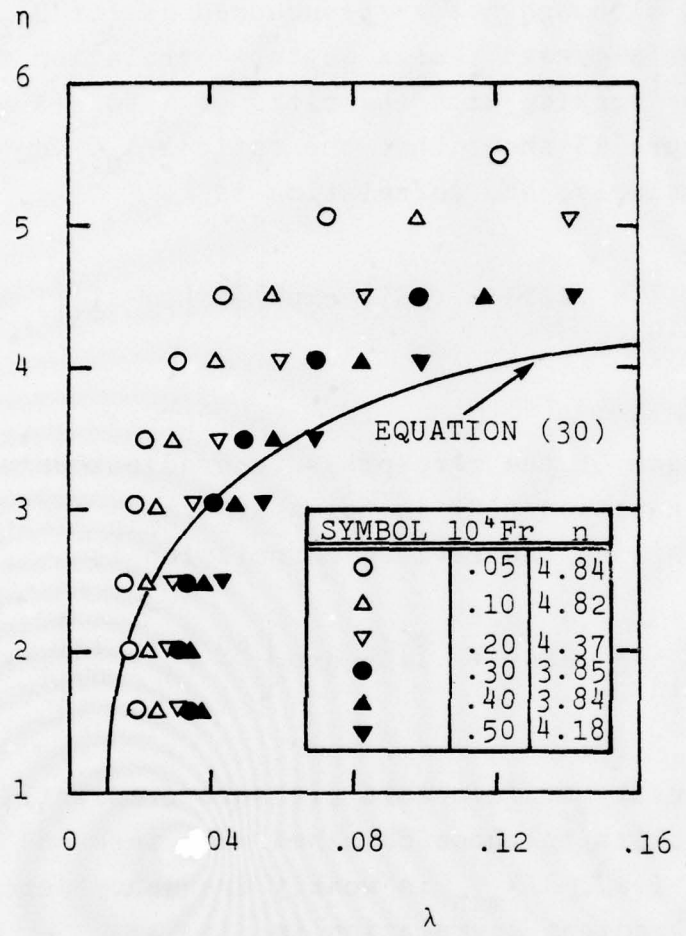

Figure 14. Profiles of the closure coefficient λ for various frequencies near the e^4-amplification point; adverse pressure gradient.

increases. Close examination of the computed results shows that the minimum value of λ increases as Fr increases. This trend is also present for zero pressure gradient (see Figure 4), although not as pronounced as for β_{FS}=-0.18. This observation suggests that a better correlation might be obtained by working with the ratio of λ to its minimum value, λ_{min}. Figure 15 shows that the ratio λ/λ_{min} does indeed correlate nicely; the correlation is

$$\frac{\lambda}{\lambda_{min}} = .9488 + .0512 \exp\left[\frac{43}{4}\left(\frac{y}{\delta} - \frac{1}{4}\right)\right]; \quad \beta_{FS} = -.18 \tag{45}$$

Reexamination of the zero-pressure-gradient data shows that rewriting Equation (30) in terms of λ/λ_{min} and y/δ improves the correlation; the revised correlation is

$$\frac{\lambda}{\lambda_{min}} = .8564 + .1436 \exp\left[\frac{60}{7}\left(\frac{y}{\delta} - \frac{1}{6}\right)\right]; \quad \beta_{FS} = 0 \tag{46}$$

Turning finally to favorable pressure gradient, we find similar results to those obtained with zero and adverse gradients, i.e., λ/λ_{min} is weakly frequency dependent. The favorable gradient correlation is

$$\frac{\lambda}{\lambda_{min}} = .604 + .396 \exp\left[\frac{48}{7}\left(\frac{y}{\delta} - \frac{1}{6}\right)\right]; \quad \beta_{FS} = +.18 \tag{47}$$

Figure 16 displays the three inferred λ/λ_{min} profiles defined in Equations (45)-(47).

As a final comment, examination of the computed values of λ_{min} shows that an excellent correlation of λ_{min} can be

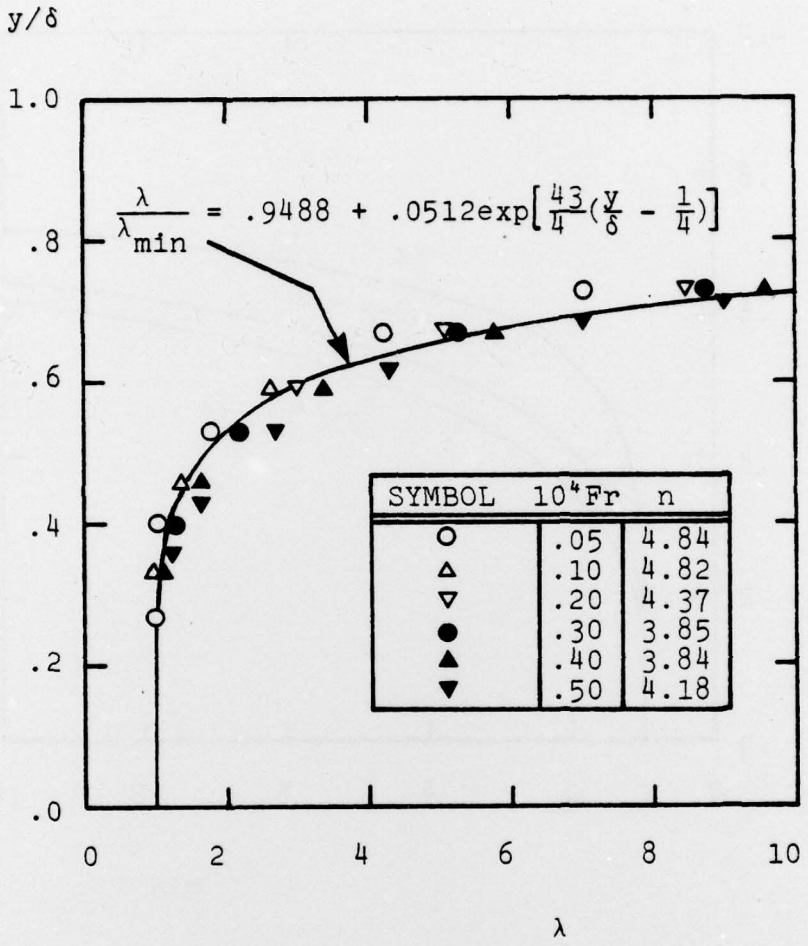

Figure 15. Correlation of λ/λ_{min} with adverse pressure gradient.

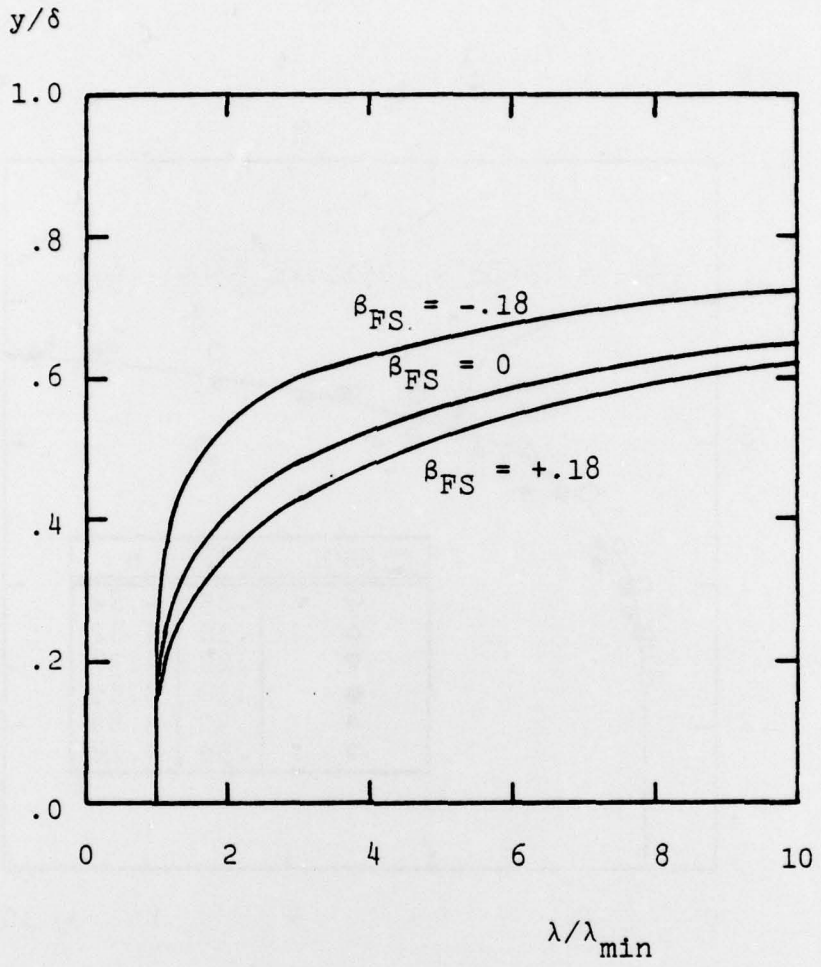

Figure 16. Inferred profiles of λ/λ_{min} for the three pressure gradients.

devised which is independent of pressure gradient. Specifically, λ_{min} is found to vary inversely with displacement-thickness Reynolds number, Re_{δ^*}, according to the following formula:

$$\lambda_{min} = 38/Re_{\delta^*} \qquad (48)$$

Figure 17 compares computed values of λ_{min} with Equation (48).

4.2 BOUNDARY CONDITIONS

As the initial profiles appear to have little effect on transition predictions attending use of the established procedure, we now proceed directly to boundary conditions. Again we use Equation (34) to define the boundary-layer edge value of the turbulent mixing energy. Also, Equation (37) remains valid for determining ω_e/ω_{e_0} although the validity of Equation (35) must be ascertained.

Figure 18 shows computed values of $\nu\omega_{e_0}/U_e^2$ as a function of Fr for favorable, zero and adverse pressure gradients. As in the $\beta_{FS}=0$ case, we find that $\nu\omega_{e_0}/U_e^2$ is proportional to $Fr^{7/4}$. Furthermore, the following modified relation correlates all of the data to within a few percent.

$$\frac{\nu\omega_{e_0}}{U_e^2} = 28\ Fr^{7/4} \qquad (49)$$

Hence, even in the presence of pressure gradient, the edge value of ω is uniquely determined as a function of the frequency of the disturbance.

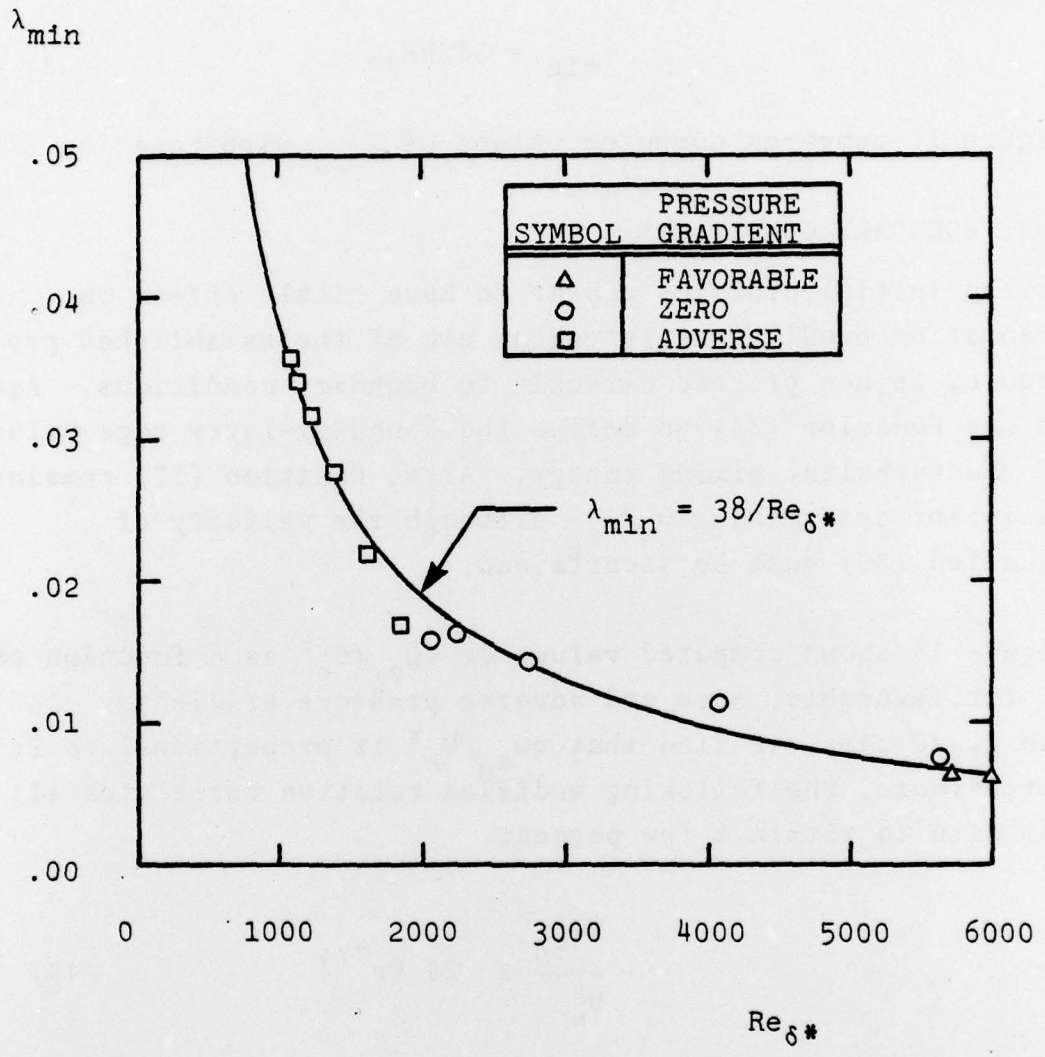

Figure 17. Correlation of λ_{min} as a function of displacement thickness Reynolds number, $Re_{\delta*}$.

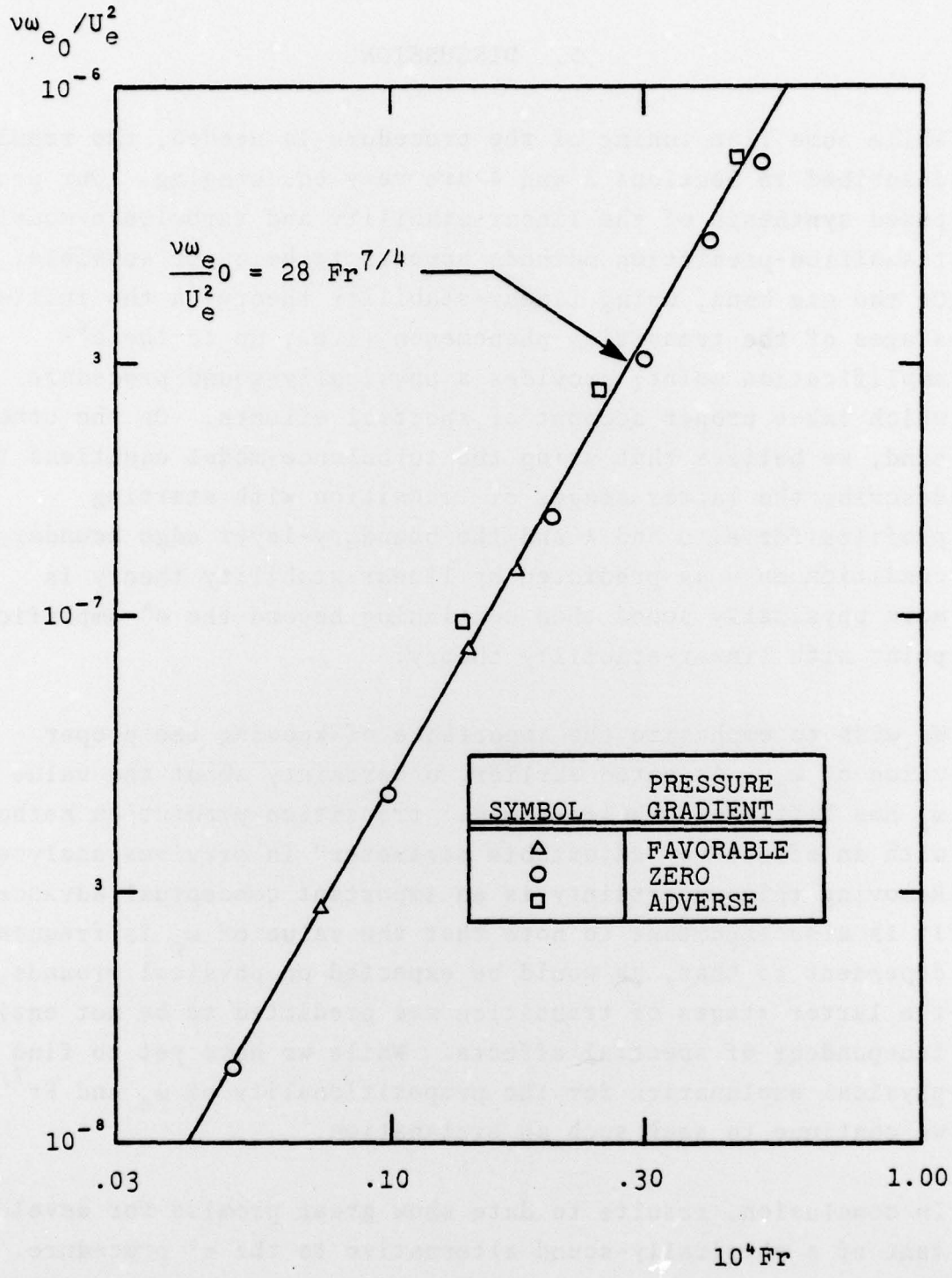

Figure 18. Correlation of boundary-layer-edge value of the turbulent dissipation rate with dimensionless frequency Fr for all pressure gradients.

5. DISCUSSION

While some fine tuning of the procedure is needed, the results described in Sections 3 and 4 are very encouraging. Our proposed synthesis of the linear-stability and turbulence-model transition-prediction methods appears to be quite sensible. On the one hand, using linear-stability theory in the initial stages of the transition phenomenon (i.e., up to the e^4-amplification point) provides a physically-sound procedure which takes proper account of spectral effects. On the other hand, we believe that using the turbulence-model equations to describe the latter stages of transition with starting profiles for e, ω and λ and the boundary-layer edge boundary condition on ω as predicted by linear-stability theory is more physically sound than continuing beyond the e^4-amplification point with linear-stability theory.

We wish to emphasize the importance of knowing the proper value of ω_e. As noted earlier, uncertainty about the value of ω_e has left the turbulence-model transition-prediction method with an effective "adjustable parameter" in previous analyses. Removing this uncertainty is an important conceptual advance. It is also important to note that the value of ω_e is frequency dependent so that, as would be expected on physical grounds, the latter stages of transition are predicted to be not entirely independent of spectral effects. While we have yet to find a physical explanation for the propositionality of ω_e and $Fr^{7/4}$, we continue to seek such an explanation.

In conclusion, results to date show great promise for development of a physically-sound alternative to the e^9 procedure. Further research should be conducted to determine how well the method predicts transition-point location for well-documented flows with adverse and/or favorable pressure gradient. Also,

further testing is needed to more definitively establish the method's sensitivity to the point of initiation of the turbulence-model phase of the computation. When such analyses have been done we feel confident a reliable analytical tool for predicting boundary-layer transition will result.

REFERENCES

1. Smith, A.M.O. and Gamberoni, N., "Transition, Pressure Gradient, and Stability Theory," Report ES 26388, Douglas Aircraft Co., Inc., El Segundo, CA (1956).

2. Van Ingen, J.L., "A Suggested Semi-Empirical Method for the Calculation of the Boundary Layer Transition Region," Dept. Aero Eng., Inst. of Technology, Delft, Report V.T.H. 74 (1956).

3. Mack, L.M., "Transition and Laminar Instability," JPL Publication 77-15 (May 1977).

4. Wilcox, D.C., "Research on the Post-Critical Stages of Transition," Report ONR-CR289-020-1F (Jan. 1978).

5. Wilcox, D.C. and Traci, R.M., "A Complete Model of Turbulence," AIAA Paper 76-351 (Jul. 1976).

6. Wilcox, D.C., "A Model for Transitional Flows," AIAA Paper 77-126 (Jan. 1977).

7. Wilcox, D.C. and Chambers, T.L., "Streamline Curvature Effects on Turbulent Boundary Layers," AIAA Journal, Vol 15, No 4, pp 574-580 (Apr. 1977).

8. Schubauer, G.B. and Skramstad, H.K., "Laminar Boundary-Layer Oscillations and Transition on a Flat Plate," NACA 909 (1948).

LIST OF SYMBOLS

SYMBOL	DEFINITION
e	Turbulent mixing energy defined in Equation (13)
f	Dimensionless streamfunction
Fr	Dimensionless frequency, $\nu\hat{\omega}/U_e^2$
m	Falkner-Skan profile parameter
p	Static pressure
R	Plate-length Reynolds number
Re_T	Turbulent Reynolds number defined in Equation (8)
$Re_{\theta t}$	Transition Reynolds number based on momentum thickness
Re_{δ^*}	Reynolds number based on displacement thickness
t	Time
T'	Freestream turbulence intensity
u,v,w	Velocity components in x,y,z directions
U_∞	Freestream velocity
U_e	Boundary-layer-edge velocity
x,y,z	Cartesian coordinates in streamwise, normal, lateral directions
α,α^*	Closure coefficients
$\hat{\alpha}$	Complex wave number
β,β^*	Closure coefficients
$\hat{\beta}$	Complex wavenumber
β_{FS}	Falkner-Skan profile parameter
δ	Boundary-layer thickness
ε	Kinematic eddy viscosity
η	Blasius similarity variable
$\tilde{\eta}$	Falkner-Skan similarity variable
λ	Closure coefficient
$\overline{\lambda}$	Average value of λ defined in Equation (31)
λ_{min}	Minimum value of λ
ν	Kinematic molecular viscosity
$\pi(y)$	Complex pressure eigenfunction
ρ	Density
σ,σ^*	Closure coefficients

LIST OF SYMBOLS

SYMBOL	DEFINITION
$\phi(y)$	Complex normal-velocity eigenfunction
Φ	Dimensionless dissipation-rate function defined in Equation (33)
ω	Turbulent dissipation rate defined in Equation (14)
ω	Frequency
ℓ	Turbulent length scale, $e^{\frac{1}{2}}/\omega$

Subscripts and Superscripts

e	Boundary-layer-edge value
i	Imaginary part
r	Real part

Other Notation

For a given variable ψ:

$\langle\psi\rangle$	Long-time-averaged value of ψ defined in Equation (20)
ψ'	Fluctuating part of ψ

DISTRIBUTION LIST

Chief of Naval Research
Department of the Navy
Arlington, VA 22217
- ONR Code 211 — 5
- ONR Code 222 — 1
- ONR Code 438 — 1

Chief of Naval Development
Department of the Navy
Washington, DC 20360
- NAVMAT 0331 — 1

Naval Sea Systems Command
Washington, DC 20362
- Code 09GS (Library) — 1

Naval Sea Systems Command
Washington, DC 20362
- Dr. T. Pierce, Code 03512 — 1

David Taylor Naval Ship Research and Development Center
Bethesda, MD 20084
- Code 16 — 1
- Code 19 — 1
- Code 154 — 1

Naval Research Laboratory
Washington, DC 20375
- Technical Information Office Code 2627 — 1
- Library, Code 2629 — 1
- Code 8441 (Dr. J. Hansen) — 1

Superintendent
U. S. Naval Academy
Annapolis, MD 21402 — 1

Superintendent
U. S. Naval Postgraduate School
Monterey, CA 93940 — 1

Director
Office of Naval Research Branch Office
495 Summer St.
Boston, MA 02210 — 1

Director
Office of Naval Research Branch Office
536 South Clark St.
Chicago, IL 60605 — 1

Director
Office of Naval Research Branch Office
1030 E. Green St.
Pasadena, CA 91106 — 1

Technical Library
Naval Coastal Systems Laboratory
Panama City, FL 32401 — 1

Defense Documentation Center
Cameron Station
Alexandria, VA 22314 — 12

Naval Underwater Systems Center
Newport, RI 02840
- Code SB 323 — 1

Air Force Office of Scientific Research
Bldg. 410
Bolling AFB, DC 20332
- Aerospace Sciences (NA) — 1

Army Research Office
P. O. Box 12211
Research Triangle Park, NC 27709
- Dr. R. Singleton — 1

National Aeronautics and Space Administration
Langley Research Center
Hampton, VA 23665
- Dr. D. Bushnell — 1

Lockheed Missiles & Space Co., Inc.
Huntsville Research & Engineering Ctr.
P. O. Box 1103
Huntsville, AL 35807
- Mr. A. Zalay — 1

General Dynamics/Convair Div.
Kearny Mesa Plant
P. O. Box 80847
San Diego, CA 92138
Dr. E. Levinsky 1

Flow Research Company
P. O. Box 5040
Kent, WA 98031
Dr. E. Murmann 1

Dynamics Technology, Inc.
3838 Carson Street
Suite 110
Torrance, CA 90503
Dr. Denny Ko 1

Advanced Technology Center, Inc.
P. O. Box 6144
Dallas, TX 75222
Dr. C. Haight 1

Massachusetts Institute of Technology
Department of Ocean Engineering
Cambridge, MA 02139
Prof. P. Leehey 1

Massachusetts Institute of Technology
Department of Aeronautics and Astronautics
Cambridge, MA 02139
Prof. M. Landahl 1

Graduate Aeronautical Laboratories
California Institute of Technology
Pasadena, CA 91125
Prof. H. W. Liepmann 1

Rand Corporation
1700 Main Street
Santa Monica, CA 90406
Dr. W. S. King 1

Case Western Reserve University
Dept. of Fluid, Thermal and Aerospace Sciences
Cleveland, OH 44106
Prof. E. Reshotko 1

Illinois Institute of Technology
Dept. of Mechanics and Mechanical and Aerospace Engineering
3300 South Federal Street
Chicago, IL 60616
Dr. Mark V. Morkovin 1

University of Southern California
Dept. of Aerospace Engineering
University Park
Los Angeles, CA 90007
Prof. John Laufer 1

Virginia Polytechnic Institute and State University
Dept. of Engineering Science and Mechanics
Blacksburg, VA 24061
Prof. A. H. Nayfeh 1

California State University, Long Beach
Dept. of Mechanical Engineering
Long Beach, CA 90840
Prof. T. Cebeci 1

Cambridge Hydrodynamics Laboratory
54 Baskin Road
Lexington, MA 02173
Dr. S. A. Orszag 1

Jet Propulsion Laboratory
4800 Oak Grove Drive
Pasadena, CA 91103
Mr. Leslie M. Mack 1